Shear Localization and Microstructure in Coarse Grained Beta Titanium Alloy

Bingfeng Wang, Xiaoyan Wang, Zezhou Li, Rui Ma, Shiteng Zhao, Fangyu Xie, Xiaoyong Zhang

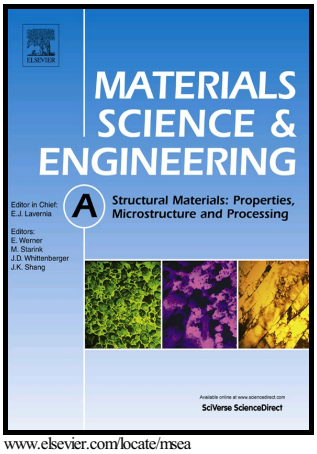

www.elsevier.com/locate/msea

PII: S0921-5093(15)30686-9
DOI: http://dx.doi.org/10.1016/j.msea.2015.11.102
Reference: MSA33084

To appear in: *Materials Science & Engineering A*

Received date: 28 September 2015
Revised date: 30 November 2015
Accepted date: 30 November 2015

Cite this article as: Bingfeng Wang, Xiaoyan Wang, Zezhou Li, Rui Ma, Shiteng Zhao, Fangyu Xie and Xiaoyong Zhang, Shear Localization and Microstructur in Coarse Grained Beta Titanium Alloy, *Materials Science & Engineering A* http://dx.doi.org/10.1016/j.msea.2015.11.102

Shear Localization and Microstructure in Coarse Grained Beta Titanium Alloy

Bingfeng Wang[1, 2, 3, 4]*, Xiaoyan Wang [1, 2], Zezhou Li [3], Rui Ma [2], Shiteng Zhao [3], Fangyu Xie [1, 2], Xiaoyong Zhang [1]

1. State Key Laboratory for Powder Metallurgy, Central South University, Changsha, Hunan, People's Republic of China;

2. School of Materials Science and Engineering, Central South University, Changsha, Hunan, People's Republic of China;

3. Department of Mechanical and Aerospace Engineering, University of California, San Diego, United States of American;

4. Key Lab of Nonferrous Materials, Ministry of Education, Central South University, Changsha, Hunan, People's Republic of China;

*Corresponding author.

Tel.: +1-(858) 900-6320, +86-731-88876244;

E-mail: biw009@ucsd.edu, wangbingfeng@csu.edu.cn

Postal address: School of Materials Science and Engineering, Central South University, Changsha 410083, Hunan, People's Republic of China

Abstract

Adiabatic shear localization plays an important role in the deformation and failure of the coarse grained beta titanium alloy Ti - 5 Al - 5 Mo - 5 V - 1 Cr - 1 Fe with grain size about 1 mm at high strain rate deformation. Hat shaped specimens with different nominal shear strains are used to induce the formation of shear bands under the controlled shock-loading experiments. The true stress in the specimens can reach about 1040 MPa where the strain is about 1.83. The whole shear localization process lasts about 35 microseconds. The microstructures within the shear band are investigated by optical microscopy, scanning electron microscopy / electron backscatter diffraction, and transmission electron microscopy. The results show that the width of the shear bands decreases with increasing nominal shear strain, and the

grains in the transition region near the shear band are elongated along the shear band, and the core of the shear band consists of the ultrafine deformed grains with width of 0.1 micron and heavy dislocations. With the aims of accommodating the imposed shear strain and maintaining neighboring grain compatibility, the grain subdivision continues to take place within the band. A fiber texture is formed in the core of the shear band. The calculated temperature rise in the shear band can reach about 722 K. Dynamic recovery is responsible for the formation of the microstructure in coarse grained beta titanium alloy.

Keyword: EBSD; Titanium alloys; Bulk deformation; Shear bands; Grain refinement;

1. Introduction

Titanium alloys are often used in aerospace industries due to their best combination of the high strength-to-weight ratio and outstanding resistance to fatigue, high temperature and environmental effects [1-2]. Compared with alpha and alpha-beta titanium alloys, beta alloys have higher yield strength and better fatigue and crack propagation properties. Thus, considerable attention is now focused on the development and application of beta titanium alloys [3-5]. Ti – 5 Al – 5 Mo – 5 V – 1 Cr – 1 Fe (Ti-55511), a type of near beta titanium alloy, has been widely applied to fabricate load-bearing parts in the aerospace industry, e.g. aircraft landing gears which always suffer dynamic fatigue and fracture [6].

Many documented researches investigated the static and quasi-static deformation of monocrystal and coarse grained metals, such as Cu, Al, steel, and Ti alloy [7 - 11]. The absence of the defects associated with grain boundaries in the monocrystalline solid and coarse grained materials give monocrystals unique properties, particularly mechanical, optical and electrical properties [7]. Groh et al. [8] proposed a crystal plasticity model to predict the mechanical response of an aluminum single crystal deformed under uniaxial compressive loading. Semboshi et al. [9] studied the microstructure and hardness of a single-crystal Cu-4 mol% Ti alloy aged at 723 K.

Karaman et al. [10] also studied the deformation of single crystals Hadfield steel for selected crystallographic orientations under tension and compression. A study on Ti - 10 V - 2 Fe - 3 Al with single phase beta microstructure reported that fracture toughness follows a similar relation to grain size as Hall-Petch relation [11]. The dynamic mechanical properties of materials related to the high strain rate are important for material applications [12]. More attentions should be paid to the deformation of monocrystal and coarse grained materials under the high strain rate loading.

Shear localizations are often observed in titanium alloys when subjected to dynamic loading due to the properties of low heat conductivity and high adiabatic shearing sensitivity [13-16]. Adiabatic shear band is a typical material phenomenon associated with shear localization, and also an important precursor to dynamic failure [17-18]. The evolution of shear localization is a rapid, progressive process during which the localization becomes more apparent and the width of the band becomes gradually narrower with the growth of shear stress. This can be rationalized in terms of the Bai -Dodd's and Grady's equations to predict the width of shear-bands [19-20]. However, the study of Pérez-Prado et al. [14] on the width of the shear bands in tantalum alloys certified that the width is related to the experimental shear strain and strength. The relationship of the experimental shear strain, the grain size of the specimen with the width of the shear band is still not clear now.

Formation of the microstructure in the shear band is a hot topic in the materials science. It is found that the microstructure of the shear band is different from the matrix, and the fine substructure may be attribute to a wide range of mechanisms, such as dynamic recovery [14, 21], recrystallization [22 - 24], and amorphization [25]. Several classical nucleation mechanisms for recrystallization have been proposed and examined. It takes much more time for the recrystallized grains to form in the shear band [22-24]. Thus, the classical recrystallization models could not account for all microstructural evolution in the shear bands. A rotational grain boundary mechanism

for recrystallization proposed by Meyers et al. [26] can be used to explain the formation of ultrafine grains in the shear band in a short instant. However, Perez-Prado 's results [14] on Ta and Ta –10 W alloys suggested that the evolved temperature in the shear band was not above the recrystallization temperature of these materials, meanwhile TEM analysis of the shear bands in these materials also indicates that no recrystallized grains exist, thus, dynamic recovery was occurring within these shear bands.

The aims of this paper are (1) to investigate the localized plastic deformation of coarse grained beta titanium alloy under controlled dynamic compressive loading, thus obtaining the mechanical response and the microstructure in the shear band, (2) to discuss the relationship of the nominal strain and strength with the width of shear band in coarse grained titanium alloy, and (3) to discuss the microstructure and microtexture evolution in the shear band, especially the formation mechanism of the shear band.

2. Experimental and Procedures

The as received metastable beta alloy Ti - 5 Al - 5 Mo - 5 V - 1 Cr - 1 Fe (Ti - 55511) [13] was solution treated at 890 ℃ for 1.5 hours, followed by water quenching to obtain beta phase grains, where solution treatment was performed above the beta - transus temperature (850 ℃) [27]. Fig. 1(a) and Fig. 1 (b) show the microstructure and the X-ray diffraction spectra of the material after the solution treatment, respectively. Thus, the material used in this study is coarse grained beta titanium alloy with grain sizes about 1 mm.

The hat-shaped specimen, originally concerned by Meyer and Manwaring [28], was used to produce a shear band in the Ti-55511 alloy at high strain rate under controlled dynamic impact compression conditions (Fig. 2). The thickness of the designed shear zone in hat-shaped specimen is about 0.5 mm.

Nominal shear strain is equal to the shear displacement divided by the thickness of the designed shear zone [29].

$$\gamma_{nominal} = \frac{shear\ displacement}{shear\ zone\ thickness} \quad (1)$$

Four specimens with nominal shear strains ($\gamma_{nominal}$) of 1.64, 1.8, 2.52, and 2.63 were conducted using a split Hopkinson pressure bar at 293 K. Details of the dynamic testing have been described elsewhere [30].

The shear stress, the strain rate, the shear strain and the true stress applied to the shear band in the specimen were calculated from data collected by the strain gauges on the incident and transmitted bars, as the following equations [31, 32].

$$\tau = \frac{E_0 A_s \varepsilon_t(t)}{\pi h(\frac{d_i + d_e}{2})} \quad (2)$$

$$\dot{\gamma} = \frac{2C_0\left[(\varepsilon_i(t) - \varepsilon_t(t)\right]}{s} \quad (3)$$

$$\gamma = \frac{2C_0\int_0^t\left[(\varepsilon_i(t) - \varepsilon_t(t)\right]dt}{s} \quad (4)$$

$$\sigma = 2\tau \quad (5)$$

where E_0 and C_0 are elastic modulus and elastic wave speed in the split Hopkinson pressure bar; A_s is the cross section area of the bar; h and s are the thickness of the designed shear zone and the width of the shear band; d_i and d_e are the geometrical parameters of the hat-shaped specimen; $\varepsilon_i(t)$ and $\varepsilon_t(t)$ are the experimentally measured strain of incident and transmitted stress pulse on the split Hopkinson pressure bars, respectively.

Culver [33] introduced a simple relation between the true strain (ε) and the shear strain (γ) expressed as Eq. (6).

$$\varepsilon = \ln\sqrt{1 + \gamma + \frac{\gamma^2}{2}} \quad (6)$$

The samples for investigation were cut from the hat-shaped specimens by electrical discharge machining. The sectioned surfaces were polished and etched by 1 ml hydrofluoric acid + 3 ml nitric acid + 80 ml water. Optical microscopy (OM) was performed with POLYVAR-MET. Scanning electron microscopy (SEM) observations

were carried out with a FEI Quanta-200 scanning electron microscope operated at 20 kV. The samples were reduced to a thickness of about 0.06 mm by polishing, and then the foils were perforated upon the shear band by electro-polishing in the solution of 300 ml methanol + 175 ml 1-butanol + 30 ml perchloric acid at 243 K. TEM observations were performed using a Tecnai G^2 F20 transmission electron microscope operated at 200 kV. The EBSD measurements were carried out using FEI Quanta 200 scanning electron microscope operated at 20 kV, and the statistic orientation analysis were carried out using Orientation Imaging Microscopy (OIM) TSL software.

3. Results and discussion

3.1 Mechanical responses of the specimens

Fig. 3(a) shows the relationship between voltage pulse and loading time during the split Hopkinson press bar experiment. The strain rate during shear deformation can be calculated from the relationship between voltage pulse and loading time under the controlled dynamic testing (Fig. 3(a)) and Eq. (3), as shown in Fig. 3(b). Thus, the specimen ($\gamma_{nominal}$ = 1.64) was tested at the strain rate about 2.4×10^5 s^{-1}. The adiabatic shearing deformation starts from the first peak value of the strain rate to the last loading stress peak [31]. Therefore, it is found that the shear deformation process of the specimen ($\gamma_{nominal}$ = 1.64) lasts for about 35 microseconds.

The relation of the true flow stress and the true strain in the shear band can be obtained using Eqs. (2) - (6), as shown in Fig. 3(c). This curve demonstrates the deformation process of the coarse grained beta titanium alloy during the shear localization. It could be divided into three stages (Fig. 3(c)). In the first stage (a - b), the true flow stress increases with the true strain due to strain hardening and strain rate hardening, and the true flow stress reaches the maximum value of 1040 MPa where the strain is about 1.83. Beyond the maximum flow stress, in the second stage (b - c), thermal softening begins to play a major role in the deformation process. Consequently, the flow stress decreases progressively with further increase in strain, which represents the start of unstable deformation, i.e. shear localization. In the last

stage (c - d), the true stress sharply decreases as the strain increases for the reason that the effect of the thermal softening is more and more remarkable, and the thermoviscoplastic instability commences.

3.2 Width of the shear bands

Fig. 4 shows optical micrographs of the shear bands in the specimens with nominal shear strains of 1.64, 1.80, and 2.52. It can be seen that the white-etching shear bands are formed in these specimens, and they are long and straight bands distinguished from the matrix, and the matrix grains are transformed into the long strip structure nearly perpendicular to the shear band. The width of the shear bands in specimens with nominal shear strain of 1.64, 1.80, and 2.52 are 24.53 microns, 23.54 microns, and 21.83 microns, respectively. When the nominal shear strain reaches 2.63, the specimen is broken. Therefore, the width of the shear band decreases with increasing nominal shear strain within a given alloy.

Bai and Dodd [19] proposed a physical model to evaluate the half width of the shear band, as follows.

$$\delta_{1/2} = \sqrt{\frac{KT}{\beta_T \dot{\gamma}}} \bullet \tau^{-\frac{1}{2}} \tag{7}$$

where τ and $\dot{\gamma}$ are the shear stress and strain rate, β_T is the fraction of plastic energy converted to heat, commonly $\beta_T = 0.9$, T is the temperature rise in the band, ρ is the material density, C is the heat capacity, and K is thermal conductivity coefficient, respectively. The parameters for Ti-55511 used in Eq. (7) are as follows ρ = 4620 kg/m^3, C = 523 J/(kg*K) [34].

Grady [20] considered the thermal softening term and proposed another physic model to predict the width of the shear band.

$$\delta = \left(\frac{9\rho^3 c^2 x^3}{\tau^3 \alpha^2 \dot{\gamma}} \right)^{1/4} \tag{8}$$

where α is the thermal softening rate, χ is the thermal diffusion coefficient. For Ti-55511, $\alpha = 7.1\times10^{-4}$ K^{-1}, $\chi = 7.16\times10^{-4}$ m^2/s [20].

Fig. 5 shows the width of the shear bands obtained from experiments as compared to the prediction by Bai-Dodd's and Grady's equations. The trend of the measured width of the shear bands in the coarse grained titanium alloy parallels the two equations, and the measured data are close to the calculated results of Bai-Dodd's equation. Thus, the effect of the thermal softening on the width of the shear band in this titanium alloy may not obvious as it in the other fine grained materials for the reason of the coarse grain size.

We measured the width of the shear bands in the fine grained Ti-55511 alloys [35] and plotted them in Fig. 5. A comparison between two grain sizes indicates that the fine grained alloy produced narrower shear regions relative to the coarse grained one. That's because the smaller the grain size, the greater the stress and higher strengths in materials generally result in an increased tendency for strain localization which is consistent with the results of Bai-Dodd and Grady.

3.3 Microstructure in the shear band

Fig. 6 shows the shear band in the specimen ($\gamma_{nominal} = 1.64$). The formation of the shear band affects the microstructure in the coarse grained grain, and a mass of feather structure formed in it. Larger magnification of bright field electron microscopy observations can be showed in Fig. 7. It can be recognized that the substructure in the boundary of the shear band consists of highly-elongated dislocation cells. In the core of the shear band, there are a number of ultafine deformed grains with width of 0.1 micron, and the microstructure is not recrystallized one due to the fact that the boundaries present are heavily dislocated, not refined and relatively unfaceted (Fig.7 (b)-(d)).

EBSD measurements have been performed to measure the local orientations of grains within the shear bands and in a region adjacent to them. The microtexture of the grains in the whole localized shear region is illustrated in Fig. 8. The white regions in the center of the Orientation Imaging Microscopy (OIM) map in Fig. 8(a) are areas where no orientation data could be acquired. This could be due to the presence of a

large density of dislocations or of a very fine microstructure, a smaller scale than the resolution limit of EBSD (ca. 0.2 micron). The shear band is located at the center of the OIM map, and the reference system is taken so that the shear plane normal (SPN) and the shear direction (SD) are approximately parallel to x- and y-axes of the figure, respectively, shown in Fig.8(a). Grain subdivision on approaching the shear band can be clearly appreciated. Hansen and Liu and coworkers [36 - 38] have classified deformation induced boundaries into incidental dislocation boundaries (IDBs) and geometrically necessary boundaries (GNBs). Boundaries resulting from grain subdivision are presumed to be GNBs since, as will be shown later, they have rather large misorientations and the separated regions undergoing independent rotations. Grains were subdivided in order to be able to accommodate the imposed shear strain. Lattice rotation was followed along several paths in the microstructure, depicted in Fig. 8 (b-d). The paths in Figs. 8 (b, c) run respectively inclined and perpendicular to the shear band, whereas the path depicted in Fig. 8 (d) runs parallel to it. The lattice rotation within a (sub) grain (region separated by two deformation induced boundaries) is small (Fig. 8 (b)), whereas significant lattice rotations can be observed when traversing along several (sub) grains (Fig. 8(c-d)) that initially belonged to the same grain. The point-to-point misorientations are plotted versus distance along path A in Fig. 8(a), as shown in Fig. 9. Misorientations up to 60° can be observed. Hughes and Hansen [38] observed and modeled grain subdivision into crystallites having large misorientations. They attributed this to the fact that different portions of a grain rotate at different rates and with different rotation axes, resulting in large differences in orientation. The results reported herein are fully consistent with their grain subdivision mechanism. Fig. 8(e) shows the microtexture data corresponding to the core of the shear band. Orientation data were acquired in isolated locations (region E). It suggests that grain subdivision continues to take place within the band, with the aim of accommodating the imposed shear strain and maintaining neighboring grain compatibility. It is interesting to note that a fiber texture is formed which is consistent

with the TEM results observed in the center of the shear band. Therefore, the imposed shear loading not only induce the shear band in the coarse grained beta titanium alloy, but also generate the ultafine deformed grains in the shear band. The examination of the texture evolution reflects the fact that, in addition to accommodating the imposed strain, neighboring grains also rotate and achieve compatible deformation.

3.4 Microstructure mechanism in the shear band

At high strain rates ($> 1 \times 10^3$ s^{-1}), the deformation process is extremely fast and it can be considered as an adiabatic process. Temperature rising in an adiabatic shear band associated with the deformation plays a significant role in the study of microstructure mechanism and is calculated by the following equation [26].

$$\Delta T = T - T_0 = \frac{\beta}{\rho C_V} \int_{\varepsilon_s}^{\varepsilon_e} \sigma d\varepsilon \tag{9}$$

The calculated temperature rise can be estimated by:

$$\Delta T = \frac{\beta}{\rho C_V} \sum_{i=1}^{n} S_i \tag{10}$$

$$S_i = \frac{\Delta \varepsilon_i \times (\sigma_i + \sigma_{i+1})}{2} (i = 1,2,3,..) \tag{11}$$

where T_0 is the ambient temperature, ρ is the mass density, C_V is the heat capacity, ε is the strain, σ is the stress (Fig. 3(c)), and β is the fraction of plastic energy converted to heat, commonly β = 0.9. For the Ti - 5 Al - 5 Mo - 5 V - 1 Cr - 1 Fe alloy, ρ and C_V are 4620 kg/m^3 and 523 J/ (kg·K), respectively [34]. Here, T_0 is 293 K. The relationship between the temperature and the time is displayed in Fig. 10(a), and The maximum temperatures in the shear band are about 722 K. Therefore, the temperature rise in the shear band is lower than the recrystallization for the Ti - 55511 alloy (773 K - 1043 K) [34, 39].

During the cooling process, the calculated temperature at the center of the shear band is shown in Fig. 10(b). The calculation process can be seen in our previous work [15]. It takes 15 microseconds (μs) for the shear band to cool down from maximum

temperature to ambient temperature when the shear localization ceases. The cooling rates in the shear band are calculated as high as 2.86×10^7 K/s. Therefore, the high temperature microstructure in the shear band could be preserved.

The above analysis of the mechanical responses, the microstructure and microtexture measurement in the coarse grained beta titanium alloy during the process of dynamic compressive loading suggests that the grains in the core of the shear band has been refined, and the grain boundaries in the core of the shear bands are heavily dislocated, and no dynamic recrystallization occurs in the process. Therefore, it is concluded that the titanium grains in the shear band are refined by the process of the dynamic recovery.

The width of the shear band in the coarse grained beta titanium alloy is about 20 microns, while the grain size in this alloy is about 1 mm. The shear band is across a beta titanium alloy grain, as shown in Fig. 4. A reasonable model is proposed to describe the mechanism for dynamic recovery occurring in a shear band in the coarse grained beta titanium alloy, as showed in Fig. 11. At the onset of deformation, the original grains are elongated into substructures (a); Then the original grains break up into a cell structure in order to accommodate the strain (b); With the increasing deformation the low angle boundary subgrains rotate to high angle boundaries (c); In the end, a shear band consisted of high misorientation boundary with large number of dislocation accumulated in the cell walls forms (d). This model is , in fact, in good agreement with those dynamic recovery mechanism proposed by Pérez-Prado and Hines and co-workers [14].

4. Conclusions

Coarse grained beta Ti - 5 Al - 5 Mo - 5 V - 1 Cr - 1 Fe alloy specimens with grain size 1 mm were tested by split Hopkinson pressure bar with different nominal shear strains. The true stress in the specimens can reach about 1040 MPa where the strain is about 1.83. The whole shear localization process lasts for about 35 microseconds after the first peak in stain rate - time curve. Adiabatic shear bands

formed in these titanium alloy are white-etching bands, and the matrix grains are transformed into the long strip structure nearly perpendicular to the shear band. The width of the shear bands decreases with increasing nominal shear strain. And the effect of the thermal softening on the width of the shear band in the coarse grained titanium alloy may be not obvious as it in the fine grained materials. The grain size do affect the width of the shear band, and the shear bands in the coarse grained beta titanium alloy are often thicker than that in the fine grained materials. The boundary of the shear band consists of highly-elongated dislocation cells, and the core of the shear band consists of ultrafine deformed grains with width of 0.1 micron and heavily dislocations. A fiber texture is formed in the center of the shear band. The grain subdivision continues to take place within the band with the aim of accommodating the imposed shear strain and maintaining neighboring grain compatibility. The calculated temperature rise in the shear band can reach about 722 K. Dynamic recovery takes effect on the formation of the microstructure in coarse grained beta titanium alloy.

Acknowledgments

This work was financial supported by Hunan Provincial Natural Science Foundation of China (No. 12JJ2028), and by a scholarship from the China Scholarship Council (No. 201308430093), and by the Freedom Explore Program of Central South University (No. 2015zzts175), and by State Key Laboratory of Powder Metallurgy, Central South University, Changsha, China. The authors would like to express their sincere thanks to Professor M. A. Meyers and K. S. Vecchio at UCSD for good suggestions and working environment.

References

[1] J.C. Williams, E.A. Starke Jr, Acta. Mater. 51 (2003) 5775–5799.

[2] N. Poondla, T.S. Srivatsan, A. Patnaik, M. Petraroli, J. Alloys Comp. 486 (2009) 162–167.

[3] R.R. Boyer, Mater. Sci. Eng. A 213 (1996) 103-114.

[4] K. Tokaji, J. C. Bian, T. Ogawa, M. Nakajima, Mater. Sci. Eng. A213 (1996) 86–92.

[5] R. R. Boyer, R. D. Briggs, J. Mater. Eng. Perform. 14 (2005) 681–685

[6] H. Liang, H. Guo, Y. Ning, X. Peng, C. Qin, Z. Shi, Y. Nan, Mater. Des, 63 (2014) 798–804

[7] N. Kota, O. B. Ozdoganlar, J. Manuf. Process., 14 (2012) 126-134.

[8] S. Groh, E.B. Marin, M.F. Horstemeyer, H.M. Zbib, Int. J. Plast., 25 (2009) 1456-1473

[9] S. Semboshi, E. Hinamoto, A. Iwase, Mater. Lett. 131 (2014) 90-93.

[10] I. Karaman, H. Sehitoglu, K. Gall, Y. I. Chumlyakov, H.J. Maier, Acta. Mater. 48 (2000) 1345-1359.

[11] A. Bhattacharjee, V.K. Varma, S.V. Kamat, A.K. Gogia, S. Bhargava, Metall. Mater. Trans. A 37 (2006) 1423-1433.

[12] B. Dodd, Y.L. Bai, Adiabatic Shear Localization: Frontiers and Advances, second ed. Elsevier Science Ltd. London, 2012

[13] B. F. Wang, J. Y. Sun, E. N. Hahn, X. Y. Wang, J. Mater. Eng. Perform. 24(2015) 477–483.

[14] M. T. Pérez-Prado, J. A. Hines, K. S. Vecchio, Acta. Mater. 49 (2001) 2905-2917.

[15] B. F. Wang, Z. L. Liu, X. Y. Wang, Z. Z. Li, Mater. Sci. Eng. A610 (2014) 301-308.

[16] Y. L. Bai, J. Bai, H. L. Li, F. J. Ke, M. F. Xia, Int. J. Impact. Eng., 24 (2000) 685-701.

[17] C. Zener, J. H. Hollomon, Appl. Phys. 15 (1944) 22-32.

[18] B. K. Kad, J. M. Gebert, M. T. Perez-Prado, M. E. Kassner, M. A. Meyers, Acta Mater. 54 (2006) 4111-4127.

[19] B. Dodd, Y. Bai, Mater. Sci. Technol. 5 (1989) 557-559.

[20] D. E. Grady, Mech. Mater. 17 (1994) 289-293.

[21] K. M. Cho, S. Lee, S. R. Nutt, J. Duffy, Acta Metall. Mater. 41 (1993) 923-932.

[22] M. A. Meyers, G. Subhash, B. K. Kad, L. Prasad, Mech. Mater. 17 (1994) 175-193.

[23] J. Peirs, W.Tirry, B.Amin-Ahmadi, F.Coghe, P.Verleysen, L.Rabet, D.Schryvers, J. Degrieck, Mater. Charact.75(2013)79–92.

[24] C. Z. Duan, Y. J. Cai, M. J. Wang, G. H. Li, J. Mater. Sci. 44 (2009) 897-902.

[25] N. Li, Y.D.Wang, R.L. Peng, X.Sun, P.K.Liaw, G.L.Wu, L.Wang, H.N.Cai, Acta Mater. 59 (2011) 6369–6377.

[26] M. A. Meyers, Y. B. Xu, Q. Xue, M. T. Pérez-Prado, T. R. McNelley, Acta Mater. 51 (2003) 1307-1325.

[27] K. Tokaji, J. C. Bian, T. Ogawa, M. Nakajima, Mater. Sci. Eng. A 213 (1996) 86-92.

[28] L.W. Meyer, S. Manwaring, in: L.E. Murr, K.P. Staudhammer, M.A. Meyers (Eds.), Metallurgical Applications of Shock-Wave and High-Strain-Rate Phenomena, Dekker, New York, 1986, p.657-674.

[29] U. Andrade, M. A. Meyers, K. S. Vecchio, A. H. Chokshi, Acta Metall. Mater. 42 (1994) 3183-3195.

[30] G. Sunny, F. Yuan, V. Prakash, J. Lewandowski, Exp. Mech. 49 (2009) 479-490.

[31] Q. Li, Y. B. Xu, Z. H. Lai, L. T. Shen, Y. L. Bai, Mater. Sci. Eng. A 276 (2000) 250-256.

[32] M. A. Meyers, Dynamic Behavior of Materials, Wiley-Interscience, New York, 1994.

[33] R. S. Culver, in: R. W. Rohde, B. M. Butcher, J. R. Holland (Eds.), Metallurgical Effects at High Strain Rates, Plenum Press, New York, 1973, pp. 519-523.

[34] B. Y. Huang, C. G. Li, L. K. Shi, China Material Engineering Canon, part Ⅳ, Chemical Industry Press, Beijing, 2006.

[35] B. Wang, J. Sun, X. Wang, A. Fu, Mater. Sci. Eng. A 639 (2015) 526-533.

[36] Q. Liu, N. Hansen, Scripta Metall. Mater. 32 (1995) 1289-1295.

[37] D. A. Hughes, D. C. Chrzan, Q. Liu, N. Hansen, Phys. Rev. Lett. 81 (1998) 4664-4667.

[38] D. A. Hughes, N. Hansen, Acta Mater. 45 (1997) 3871-3886.

[39] C. Li, X. Y. Zhang, Z. Y. Li, K. C. Zhou, Mater. Sci. Eng. A573 (2013) 75-83.

Figure Captions

Fig. 1 (a) Initial microstructure of coarse grained Ti-55511 alloy; (b) X-ray diffraction patterns obtained from microstructure of Fig.1(a).

Fig. 2 Schematic diagram of the hat-shaped specimen (Dimensions in mm).

Fig. 3 Dynamic responses of specimen at high strain rate: (a) Shear signals with the hat shaped specimen attached between the bars; (b) strain rate-time curves; (c) true stress - true strain curves.

Fig. 4 Optical micrographs of the shear section in the specimens. (a) for specimen H1 ($\gamma_{nominal} = 1.64$); (b) for specimen H2 ($\gamma_{nominal} = 1.80$); (c) for specimen H3 ($\gamma_{nominal} = 2.52$).

Fig. 5 The width of shear band obtained from experiments as compared to the prediction by Bai-Dodd's and Grady's equations. The shear stress obtained from experiments.

Fig. 6 Montage of the bright electron field micrographs across the shear band.

Fig. 7 Bright field electron microscopy observations of the specimen ($\gamma_{nominal} = 1.64$): (a) the microstructure in the boundary of the shear band; (b) - (d) are the microstructure in the core of the shear band.

Fig. 8 (a) OIM map showing the microstructure near the shear band; (111), (110) and (100) pole figures (b) showing the lattice rotation within a (sub)grain (path B); (c) the lattice rotation within (sub)grains along horizontal path C; (d) the lattice rotation within (sub)grains along vertical path D; (e) the lattice rotation within (sub)grains in the core of the shear band (Mark "E").

Fig. 9 Point to point misorientation along path A in Fig. 8(a)

Fig. 10 (a) Calculated temperature rise in the shear band during shear deformation; (b) calculated temperature in the shear band drop as a function of time.

Fig. 11 Schematic illustration of dynamic recovery in the shear band: (a) formation of elongate subgrains; (b) elongated grain broke into smaller subgrains; (c) rotation of subgrains; (d) high angle misorientations between some subgrains.

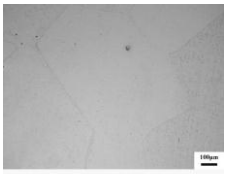

Fig. 1 (a) Initial microstructure of coarse grained Ti-55511 alloy;

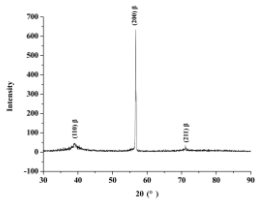

Fig.1 (b) X-ray diffraction patterns obtained from microstructure of Fig.1(a).

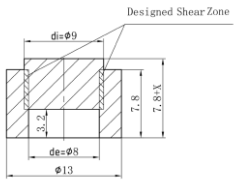

Fig. 2 Schematic diagram of the hat-shaped specimen (Dimensions in mm).

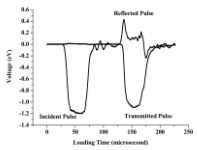

Fig. 3 Dynamic responses of specimen at high strain rate: (a) Shear signals with the hat shaped specimen attached between the bars;

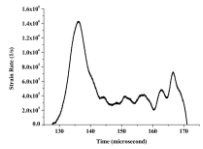

Fig. 3 Dynamic responses of specimen at high strain rate:
(b) strain rate-time curves;

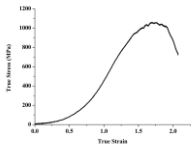

Fig. 3 Dynamic responses of specimen at high strain rate:
(c) true stress - true strain curves.

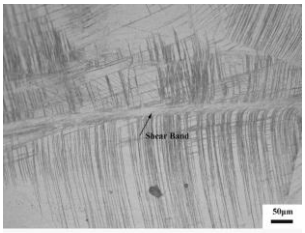

Fig. 4 Optical micrographs of the shear section in the specimens.
(a) for specimen H1 (γnominal = 1.64);

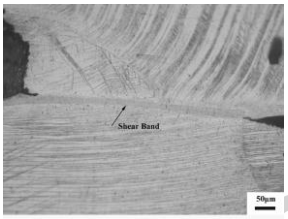

Fig. 4 Optical micrographs of the shear section in the specimens.
(b) for specimen H2 (γnominal = 1.80);

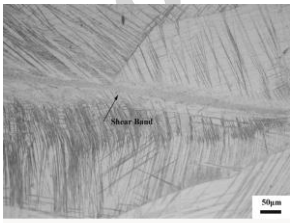

Fig. 4 Optical micrographs of the shear section in the specimens.
(c) for specimen H3 (γnominal = 2.52);

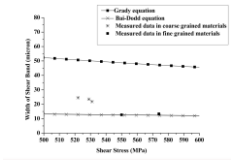

Fig. 5 The width of shear band obtained from experiments as compared to the prediction by Bai-Dodd's and Grady's equations. The shear stress obtained from experiments.

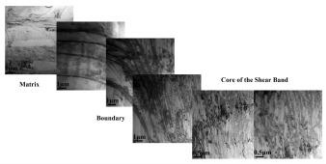

Fig. 6 Montage of the bright electron field micrographs across the shear band.

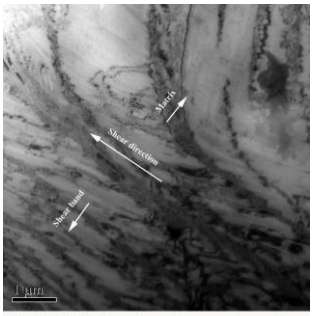

Fig. 7 Bright field electron microscopy observations of the specimen (γnominal = 1.64):
(a) the microstructure in the boundary of the shear band;

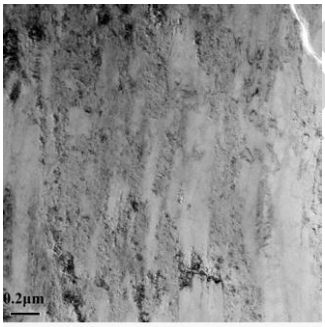

Fig. 7 Bright field electron microscopy observations of the specimen (γnominal = 1.64):
(b) the microstructure in the core of the shear band.

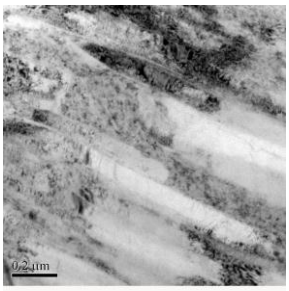

Fig. 7 Bright field electron microscopy observations of the specimen (γnominal = 1.64):
(c) the microstructure in the core of the shear band.

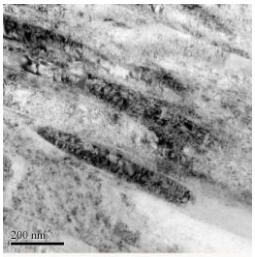

Fig. 7 Bright field electron microscopy observations of the specimen (γnominal = 1.64):
(d) the microstructure in the core of the shear band.

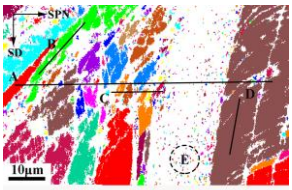

Fig. 8 (a) OIM map showing the microstructure near the shear band;

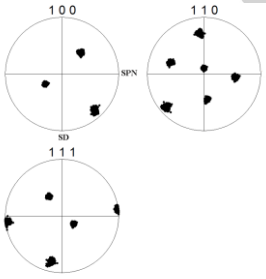

Fig. 8 (111), (110) and (100) pole figures
(b) showing the lattice rotation within a (sub)grain (path B);

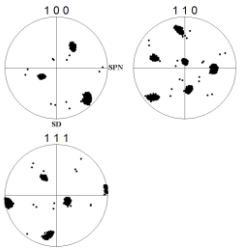

Fig. 8 (111), (110) and (100) pole figures (c) the lattice rotation within (sub)grains along horizontal path C;

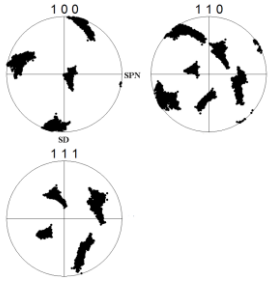

Fig. 8(111), (110) and (100) pole figures (d) the lattice rotation within (sub)grains along vertical path D;

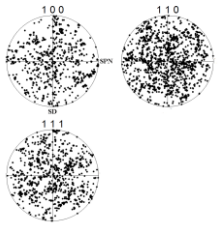

Fig. 8 (111), (110) and (100) pole figures (e) the lattice rotation within (sub)grains in the core of the shear band.

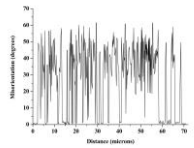

Fig. 9 Point to point misorientation along path A in Fig. 8(a)

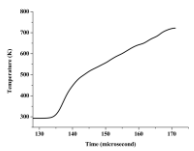

Fig. 10 (a) Calculated temperature rise in the shear band during shear deformation;

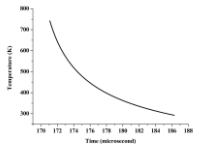

Fig. 10 (b) calculated temperature in the shear band drop as a function of time.

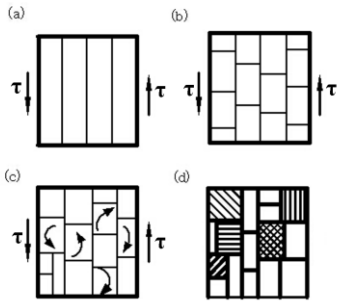

Fig. 11 Schematic illustration of dynamic recovery in the shear band: (a) formation of elongate subgrains; (b) elongated grain broke into smaller subgrains; (c) rotation of subgrains; (d) high angle misorientations between some subgrains.